Phase-matched optical second-harmonic generation in helically twisted smectic-C^* phase

I. Drevenšek Olenik and M. Čopič
Department of Physics, University of Ljubljana, Jadranska 19, 1111 Ljubljana, Slovenia
and Jožef Stefan Institute, Jamova 39, 1111 Ljubljana, Slovenia
(Received 27 January 1997)

Phase matching for optical second-harmonic generation in the helically twisted smectic-C^* liquid-crystalline phase is analyzed theoretically. Ten distinctive phase-matched combinations of the fundamental and the second-harmonic eigenmodes exist. The effective second-order nonlinear optical susceptibility and the relation between the optical wave vectors and the wave vector of helical structure are determined for each of the combinations. The results obtained within the standard approximation of the slowly varying amplitude are compared with the exact numerical solutions of the nonlinear wave equation. The discrepancy between the approximative and exact results is crucial only for the two phase-matched combinations that are realized when the second-harmonic frequency is close to the selective reflection band. In this case an additional enhancement of the second-harmonic beam can appear. [S1063-651X(97)05707-3]

PACS number(s): 42.70.Df, 42.65.Ky, 77.84.Nh

I. INTRODUCTION

The phenomenon of optical second-harmonic generation (SHG) in the ferroelectric smectic-C^* (Sm-C^*) phase has recently become very attractive from a fundamental as well as an applicable point of view. Among different SHG characteristics, the possibility for phase matching was investigated most extensively. For this purpose the spontaneously formed Sm-C^* helix was unwound by application of a static external electric field [1–9]. Phase matching in the resulting homogeneous Sm-C^* phase was then achieved by a standard technique of compensation of material color dispersion by its birefringence [10].

In addition to the standard phase-matching technique, the helical structure of the Sm-C^* phase provides some particular possibilities to achieve an efficient harmonic generation. The optical wave-vector mismatch can be compensated by the wave vector associated with the spatial periodicity of the helix. This is similar to the phenomenon of phase matching in periodically poled materials [11]. In liquid crystals such possibilities were demonstrated and analyzed by Shelton and Shen for optical third-harmonic generation (THG) in the cholesteric phase [12–14]. Later, similar features were found by Saha for the electric-field-induced SHG [15].

In this paper we study the phenomenon of optical SHG in the twisted Sm-C^* structure. The case of optical beams propagating along the helical axis is examined. The exact numerical solutions of the nonlinear wave equation are related to the analytical solutions within the standard approximation of the slowly varying amplitude. Possible phase-matched combinations of optical waves are determined and their relation to the helical periodicity of the structure is analyzed and discussed. The corresponding effective nonlinear susceptibility coefficients are found. The main similarities and differences between SHG in the Sm-C^* phase and THG or field-induced SHG in the cholesteric phase are also pointed out. In the discussion we show that our results can explain the prominent increase of the SHG signal, which has been reported by Kajikawa *et al.* [16] and Furukawa *et al.* [17] for the situation when the wavelength of the second-harmonic beam coincided with the period of the Sm-C^* helix. This particular case has already been analyzed within some approximations in our previous paper [18].

II. OPTICAL PARAMETERS OF THE Sm-C^* PHASE

The bulk ferroelectric Sm-C^* phase is characterized by a helical spatial modulation of the molecular tilt and the spontaneous electrical polarization. The direction of the modulation is normal to the smectic layers. The period of the helix, helical pitch p, is usually of the same order of magnitude as the wavelengths of the visible light. This feature has a strong influence on the optical properties of the Sm-C^* phase.

The local characteristics of the optical dielectric tensor ε and the tensor of the second-order nonlinear optical susceptibility $\chi^{(2)}$ are determined by the local C_2 symmetry of the Sm-C^* structure. In compliance with this symmetry ε has 3 and $\chi^{(2)}$ has 13 independent nonzero components. The overall permutation symmetry of the $\chi^{(2)}$ (Kleinman's symmetry) reduces the total number of its independent components to 4. This symmetry is valid when the wavelength of the fundamental and the second-harmonic optical field is far away from any absorbtion bands of the liquid crystal. In the local Cartesian system $(\vec{e}_1,\vec{e}_2,\vec{e}_3)$ oriented so that the $\vec{e}_2$ axis is parallel to the local twofold axis and the $\vec{e}_3$ axis is parallel to the principal axis of ε corresponding to the largest principal value, the nonzero components are

$$\varepsilon_{11}, \quad \varepsilon_{22}, \quad \varepsilon_{33} \tag{1}$$

and

$$\begin{gathered}\chi_{123}=\chi_{132}=\chi_{213}=\chi_{231}=\chi_{312}=\chi_{321},\\ \chi_{112}=\chi_{121}=\chi_{211},\\ \chi_{332}=\chi_{323}=\chi_{233},\\ \chi_{222}.\end{gathered} \tag{2}$$

An important optical parameter of the structure is also the angle θ between the $\vec{e}_3$ axis and the smectic layers normal, generally known as the optical tilt angle of the Sm-C^* phase.

The orientation of the local coordinate axes $(\vec{e}_1,\vec{e}_2,\vec{e}_3)$ varies in space in accordance with the helical modulation. In a fixed laboratory Cartesian system $(\vec{e}_x,\vec{e}_y,\vec{e}_z)$, with the $\vec{e}_z$ axis parallel to the smectic layers normal, the $\vec{e}_i$ are expressed in the form

$$\vec{e}_3=(\sin\theta\cos q_0z)\vec{e}_x+(\sin\theta\sin q_0z)\vec{e}_y+(\cos\theta)\vec{e}_z,$$
$$\vec{e}_2=(-\sin q_0z)\vec{e}_x+(\cos q_0z)\vec{e}_y, \tag{3}$$
$$\vec{e}_1=\vec{e}_2\times\vec{e}_3,$$

where $q_0=2\pi/p$ is the wave vector of the modulation. The components of ε and $\chi^{(2)}$ in the laboratory system are then given by

$$\varepsilon_{ij}=R_{ii'}R_{jj'}\varepsilon_{i'j'},\quad \chi_{ijk}=R_{ii'}R_{jj'}R_{kk'}\chi_{i'j'k'}, \tag{4}$$

for $i,j,k=x,y,z$ and $i',j',k'=1,2,3$, where $\mathbf{R}$ is the transformation matrix from the local to the laboratory system. The result of the transformation is given in the Appendix. From ten different components of the $\chi^{(2)}$ in the laboratory system only $\chi_{zzz}=0$, while all the others have nonzero values. The relation $\chi_{zzz}=0$ comes out because the $\vec{e}_z$ axis is everywhere perpendicular to the local twofold axis $\vec{e}_2$.

III. WAVE PROPAGATION

The process of optical SHG in the helically modulated Sm-C^* structure is governed by the nonlinear wave equation

$$\vec{\nabla}\times\vec{\nabla}\times\vec{E}(\vec{r},2\omega)-\left(\frac{2\omega}{c}\right)^2\varepsilon\vec{E}(\vec{r},2\omega)=\left(\frac{2\omega}{c}\right)^2\chi^{(2)}:\vec{E}(\vec{r},\omega)\vec{E}(\vec{r},\omega), \tag{5}$$

which describes the relation between the fundamental optical field $\vec{E}(\vec{r},\omega)$ and the second harmonic field $\vec{E}(\vec{r},2\omega)$. In typical experimental situations both fields can be considered to be plane waves and the power depletion of the fundamental beam can be neglected. Within these assumptions and taking that the fundamental beam enters the sample in the direction of the helical axis ($\vec{e}_z$ axis), the solutions of Eq. (5) can be expressed by

$$\vec{E}(\vec{r},\omega)=\sum_{k=1}^{4}A_k\vec{E}_{k,\omega}(z),$$
$$\vec{E}(\vec{r},2\omega)=\sum_{k=1}^{4}B_k(z)\vec{E}_{k,2\omega}(z), \tag{6}$$

where $\vec{E}_{k,\omega}(z)$ and $\vec{E}_{k,2\omega}(z)$ correspond to the normalized solutions of the homogeneous wave equation

$$\vec{\nabla}\times\vec{\nabla}\times\vec{E}_k(z)-\frac{\omega^2}{c^2}\varepsilon\vec{E}_k(z)=0 \tag{7}$$

at the fundamental and at the second-harmonic frequency. The amplitudes A_k are determined by the boundary conditions related to a selected experimental arrangement.

The solutions of the homogeneous wave equation (7) in the helically modulated Sm-C^* structure have been studied by different authors [19,20]. It was shown that for propagation along the helical axis the transverse component of the optical field of the eigenmodes $\vec{E}_k^{\rm tr}=\vec{E}_k-\vec{e}_z\vec{E}_k$ is analogous to the de Vries solutions for the cholesteric phase [21,22]. These are the Bloch wave fields

$$\vec{E}_k^{\rm tr}=E_{k,+}\vec{e}_++E_{k,-}\vec{e}_-=\left(\frac{-f_ke^{i(k+q_0)z}}{\sqrt{1+|f_k|^2}}\right)\left(-\frac{\vec{e}_x+i\vec{e}_y}{\sqrt{2}}\right)+\left(\frac{e^{i(k-q_0)z}}{\sqrt{1+|f_k|^2}}\right)\left(\frac{\vec{e}_x-i\vec{e}_y}{\sqrt{2}}\right), \tag{8}$$

where $\vec{e}_\pm=\mp(\vec{e}_x\pm i\vec{e}_y)/\sqrt{2}$ denote the unit vectors of the circular base. The dispersion relation $k(\omega)$ and the polarization factor f_k of these fields are given by

$$k=\pm\left((k_0^2\overline{\varepsilon}+q_0^2)\pm\sqrt{4k_0^2\overline{\varepsilon}q_0^2+\alpha^2k_0^4}\right)^{1/2} \tag{9}$$

and

$$f_k=\frac{(k-q_0)^2-k_0^2\overline{\varepsilon}}{\alpha k_0^2}=\frac{\alpha k_0^2}{(k+q_0)^2-k_0^2\overline{\varepsilon}}, \tag{10}$$

The introduced parameters k_0, $\overline{\varepsilon}$, and α are

$$k_0=\frac{\omega}{c},$$
$$\overline{\varepsilon}=\frac{1}{2}\left(\varepsilon_{11}+\varepsilon_{22}+\frac{(\varepsilon_{33}-\varepsilon_{11})\varepsilon_{11}\sin^2\theta}{\varepsilon_{11}\sin^2\theta+\varepsilon_{33}\cos^2\theta}\right), \tag{11}$$
$$\alpha=\overline{\varepsilon}-\varepsilon_{22}.$$

The longitudinal electric field of the eigenmodes is expressed as

$$E_{k,0}=\vec{e}_z\vec{E}_k=\frac{a}{\sqrt{2}}(-E_{k,+}e^{-iq_0z}+E_{k,-}e^{+iq_0z}), \tag{12}$$

where a is the tilt-dependent quantity given as

$$a=-\frac{(\varepsilon_{33}-\varepsilon_{11})\sin\theta\cos\theta}{\varepsilon_{11}\sin^2\theta+\varepsilon_{33}\cos^2\theta}. \tag{13}$$

In the SHG process the longitudinal component of the fundamental field $E_{k,0}$ contributes to the generation of the transverse component of the second-harmonic field $\vec{E}_{k,2\omega}^{\rm tr}$ and vice versa. This interaction brings some additional ''mixing'' terms to the solutions of the nonlinear wave equation (5). Such terms do not exist in the case of the cholesteric phase where $\theta=\pi/2$ and the longitudinal field vanishes.

Two of the four eigenmodes as given by Eq. (8) correspond to optical beams that propagate in the direction of the $\vec{e}_z$ axis and the other two to the equivalent beams that propagate in the direction of the $-\vec{e}_z$ axis. In the dispersion spec-

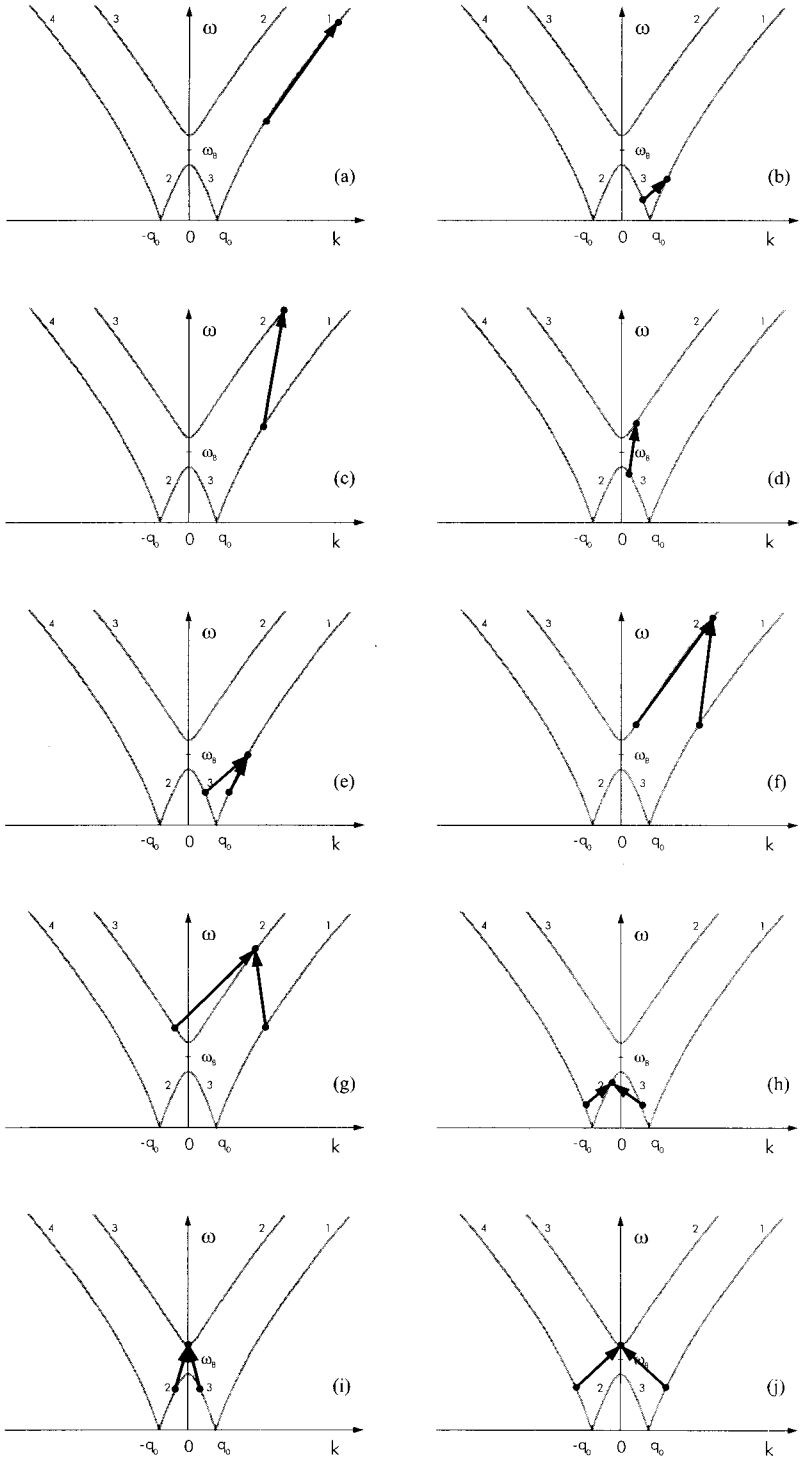

FIG. 1. Phase-matching combinations shown on the dispersion curves of the optical eigenmodes of the Sm-C^* phase. The modes corresponding to branches 1 and 2 propagate in the $\vec{e}_z$ direction, while the modes associated with branches 3 and 4 propagate in the $-\vec{e}_z$ direction. Modes 1 and 3 are polarized approximately as $\vec{e}_+$ and modes 2 and 4 as $\vec{e}_-$. This approximation breaks down when $\omega \gg \omega_B$ and for modes 2 and 3 also in the vicinity of the band gap where the modes become linearly polarized. The band-gap characterizes the region where the two values of k are imaginary and the corresponding modes are Bragg reflected from the helical structure. The symbol ω_B is used to denote the Bragg frequency $\omega_B = q_0 c/\sqrt{\varepsilon}$. The labeling of the combinations is in accordance with Table I.

trum shown in Fig. 1 the corresponding branches are labeled as branches 1,2 and 3,4 respectively. The main characteristic of the dispersion spectrum $k(\omega)$ is the gap inside which two eigenvalues of k, as found from Eq. (9), become imaginary. In the region of this gap the circularly polarized optical waves that match with the handedness of the Sm-C^* helix cannot propagate, but experience Bragg reflection from the structure.

The form (8) of the optical eigenmodes suggests that the manipulation of the nonlinear wave equation (5) would be more convenient by using the circular base $(\vec{e}_+,\vec{e}_-,\vec{e}_0)$ of the laboratory frame. Within this base the tensor of the nonlinear optical susceptibility $\chi^{(2)}$ transforms to

$$\chi_{ijk}=T_{ii'}T^*_{jj'}T^*_{kk'}\chi_{i'j'k'}, \quad i,j,k=+,-,0;$$
$$i',j',k'=x,y,z, \tag{14}$$

where the transformation matrix $\mathbf{T}$ is

$$\mathbf{T}=\begin{bmatrix} \frac{-1}{\sqrt{2}} & \frac{-i}{\sqrt{2}} & 0 \\ \frac{1}{\sqrt{2}} & \frac{-i}{\sqrt{2}} & 0 \\ 0 & 0 & 1 \end{bmatrix}. \tag{15}$$

The result of the transformation is given in the Appendix. The main benefit of using the circular base is that the four independent components of $\chi^{(2)}$ are separated. They exhibit distinctive spatial periodicities $3q_0$, $2q_0$, or q_0 with respect to the helical structure.

A. Slowly varying amplitude approximation

The standard simplification used in solving the nonlinear wave equation is the slowly varying amplitude approximation (SVAA) [23]. It assumes that in Eq. (5) the second-order derivatives of $B_k(z)$ can be neglected. In the helically modulated Sm-C^* structure the applicability of the SVAA is restricted by the condition

$$\left|\frac{\partial^2 B_k}{\partial z^2}\right| \ll \left|2[k(2\omega)\pm q_0]\,\frac{\partial B_k}{\partial z}\right| \tag{16}$$

It is evident that this condition is violated when $k(2\omega)\approx\pm q_0$, that is, when the second-harmonic frequency 2ω is much lower than the Bragg frequency $\omega_B=q_0c/\overline{\varepsilon}(2\omega)$.

Within the SVAA we get from Eq. (5) a set of two linear equations

$$\sum_k 2\left(\frac{\partial B_k}{\partial z}\right)\left(\frac{\partial \vec{E}^{\rm tr}_{k,2\omega}}{\partial z}\right)=-\left(\frac{2\omega}{c}\right)^2\sum_{k',k''}A_{k'}A_{k''}\chi^{(2)}:\vec{E}_{k',\omega}\vec{E}_{k'',\omega} \tag{17}$$

for the two eigenmodes $\vec{E}_{k,2\omega}$ that satisfy relation (16). In the circular base the set of equations (17) becomes

$$\sum_{k=\rm I,II}2\left(\frac{\partial B_k}{\partial z}\right)\left(\frac{\partial E^{2\omega}_{k,+}}{\partial z}\,\vec{e}_+ + \frac{\partial E^{2\omega}_{k,-}}{\partial z}\,\vec{e}_-\right)$$
$$=-\left(\frac{2\omega}{c}\right)^2\sum_{k',k''=1,\ldots,4}A_{k'},A_{k''}\chi^{(2)}_{\rm tr}:$$
$$\times(E^{\omega}_{k',+}\vec{e}_+ + E^{\omega}_{k',-}\vec{e}_-)(E^{\omega}_{k'',+}\vec{e}_+ + E^{\omega}_{k'',-}\vec{e}_-), \tag{18}$$

where indices I and II designate the eigenmodes at the second-harmonic frequency and the tensor of the ''transverse'' nonlinear susceptibility $\chi^{(2)}_{\rm tr}$ is defined by

$$\chi^{(2)}_{\rm tr}:\vec{E}^{\rm tr}_{k'}\vec{E}^{\rm tr}_{k''}=\chi^{(2)}:\vec{E}_{k'}\vec{E}_{k''} \tag{19}$$

The components of $\chi^{(2)}_{\rm tr}$ are calculated on the basis of the relation (12) and are explicitly given in the Appendix. By introducing $\chi^{(2)}_{\rm tr}$, both sides of Eq. (18) are expressed entirely in terms of the transverse components of the field, which simplifies further calculation and is also appropriate when considering boundary conditions at the sample surfaces.

Multiplication of Eq. (18) by $\vec{e}^*_+=-\vec{e}_-$ and $\vec{e}^*_-=-\vec{e}_+$, respectively, results in the system of two equations for $(\partial B_{\rm I}/\partial z)$ and $(\partial B_{\rm II}/\partial z)$, which is given as

$$C_k\,\frac{\partial B_k}{\partial z}=\frac{-i}{2}\left(\frac{2\omega}{c}\right)^2\sum_{k',k''=1,\ldots,4}D_{kk'k''}A_{k'}A_{k''}e^{-i[k(2\omega)-k'(\omega)-k''(\omega)]z}, \quad k=\rm I,II, \tag{20}$$

where

$$C_{\rm I}(\sqrt{1+|f_{\rm I}|^2})=(k_{\rm I}+q_0)(k_{\rm II}-q_0)f_{\rm I}-(k_{\rm I}-q_0)(k_{\rm II}+q_0)f_{\rm II}=-C_{\rm II}(\sqrt{1+|f_{\rm II}|^2}) \tag{21}$$

and

$$D_{{\rm I},k'k''}=\frac{[(k_{\rm II}+q_0)f_{\rm II}e^{iq_0z}\vec{e}^*_- +(k_{\rm II}-q_0)e^{-iq_0z}\vec{e}^*_+)]\chi_{\rm tr}:[\vec{e}_-\vec{e}_-e^{-2iq_0z}-\vec{e}_-\vec{e}_+f_{k''}-\vec{e}_+\vec{e}_-f_{k'}+\vec{e}_+\vec{e}_+f_{k'}f_{k''}e^{2iq_0z}]}{(\sqrt{1+|f_{k'}|^2})(\sqrt{1+|f_{k''}|^2})}, \tag{22}$$

$$D_{{\rm II},k'k''}=\frac{[(k_{\rm I}+q_0)f_{\rm I}e^{iq_0z}\vec{e}^*_- +(k_{\rm I}-q_0)e^{-iq_0z}\vec{e}^*_+)]\chi_{\rm tr}:[\vec{e}_-\vec{e}_-e^{-2iq_0z}-\vec{e}_-\vec{e}_+f_{k''}-\vec{e}_+\vec{e}_-f_{k'}+\vec{e}_+\vec{e}_+f_{k'}f_{k''}e^{2iq_0z}]}{(\sqrt{1+|f_{k'}|^2})(\sqrt{1+|f_{k''}|^2})},$$

Taking into account the spatial periodicities of the components $\chi_{\rm tr}$ (see the Appendix), we can see from relations (22) that the coefficients $D_{kk'k''}$ are spatially independent. They represent the effective coupling constants between various optical eigenmodes at the fundamental and second-harmonic frequency and correspond to the coefficients of the effective nonlinear optical susceptibility of the helical Sm-C^* structure.

The integration of Eq. (20) leads to the expression for the dependence of the amplitude of the SHG field

$$B_k(z)=\frac{-i}{2}\left(\frac{2\omega}{c}\right)^2\Bigg[C_k^{-1}\times\sum_{k',k''=1,\ldots,4}A_{k'}A_{k''}D_{kk'k''}z\times\frac{\sin(\Delta kz/2)}{(\Delta kz/2)}\,e^{-i\Delta kz/2}\Bigg]+F_k, \tag{23}$$

where

$$\Delta k=k(2\omega)-k'(\omega)-k''(\omega) \tag{24}$$

is the wave-vector mismatch and F_k are integration constants that are determined from boundary conditions for the second-harmonic field. For the modes propagating in the $\vec{e}_z$ direction these conditions require $\vec{E}^{\rm tr}_{k,2\omega}(z=0)=0$ and for the modes propagating in the $-\vec{e}_z$ direction they give $\vec{E}^{\rm tr}_{k,2\omega}(z=L)=0$, where L denotes the thickness of the sample. The dependence of $B_k(z)$ as given in Eq. (23) is equivalent to the dependence of the amplitude of the SHG field in optically homogeneous media (Maker oscillations) [23]. The optical inhomogeneity of the Sm-C^* structure modifies only the expression for the wave-vector mismatch Δk, which, due to the helical modulation, involves the Bloch instead of the ''usual'' wave vectors. When $\Delta k=0$ the SHG process is phase matched and the amplitude of the second-harmonic field $B_k(z)$ is increasing linear with the coordinate z.

The procedure based on the SVAA breaks down when frequency 2ω is at the reflection band edge, that is, when $k\to 0$. In this region the system of equations (18) becomes degenerate; therefore, the nonlinear wave equation (5) has to be analyzed by taking into account also the second-order derivatives $(\partial^2 B_k/\partial z^2)$. One of the ways to find the approximate analytical solutions in this case was described in our previous paper [18].

The problems with SVAA appear also when frequency 2ω is in the vicinity of the band gap. In this region, for a given fundamental field, only one of the four eigenmodes $\vec{E}_{k,2\omega}$ satisfies the inequality (16). The linearized wave equation (18) is therefore valid only for this mode. Its amplitude B_k is given by the relation

$$2\left(\frac{\partial B_k}{\partial z}\right)\left(\frac{\partial E^{2\omega}_{k,+}}{\partial z}\,\vec{e}_+ +\frac{\partial E^{2\omega}_{k,-}}{\partial z}\,\vec{e}_-\right)=-\left(\frac{2\omega}{c}\right)^2\sum_{k',k''=1,\ldots,4}A_{k'}A_{k''}\chi^{(2)}_{\rm tr}:\times(E^{\omega}_{k',+}\vec{e}_+ +E^{\omega}_{k',-}\vec{e}_-)(E^{\omega}_{k'',+}\vec{e}_+ +E^{\omega}_{k'',-}\vec{e}_-). \tag{25}$$

The multiplication of relation (25) by $\vec{e}^{\,*}_+=-\vec{e}_-$ and $\vec{e}^{\,*}_-=-\vec{e}_+$, respectively, results in two different equations for the same quantity $(\partial B_k/\partial z)$:

$$C_k+\left(\frac{\partial B_k}{\partial z}\right)=\frac{-i}{2}\left(\frac{2\omega}{c}\right)^2\sum_{k',k''=1,\ldots,4}D_{+k'k''}A_{k'}A_{k''}e^{-i\Delta kz}, \tag{26}$$

$$C_k-\left(\frac{\partial B_k}{\partial z}\right)=\frac{-i}{2}\left(\frac{2\omega}{c}\right)^2\sum_{k',k''=1,\ldots,4}D_{-k'k''}A_{k'}A_{k''}e^{-i\Delta kz}, \tag{27}$$

with the constants $C_{k\pm}$ and $D_{\pm k'k''}$ defined as

$$C_{k+}=\frac{-f_k}{\sqrt{1+|f_k|^2}}\,(k+q_0),\quad C_{k-}=\frac{1}{\sqrt{1+|f_k|^2}}\,(k-q_0), \tag{28}$$

and

$$D_{\pm k'k''}=\frac{[e^{\mp iq_0z}\vec{e}^{\,*}_{\pm}]\chi_{\rm tr}:[\vec{e}_-\vec{e}_-e^{-2iq_0z}-\vec{e}_-\vec{e}_+f_{k''}-\vec{e}_+\vec{e}_-f_{k'}+\vec{e}_+\vec{e}_+f_{k'}f_{k''}e^{2iq_0z}]}{(\sqrt{1+|f_{k'}|^2})(\sqrt{1+|f_{k''}|^2})} \tag{29}$$

The discrepancy between the solutions for the SHG field obtained on the basis of Eq. (26) or (27) might be considered as a measure for the validity of the SVAA in a particular situation. If the discrepancy is large then also the second-order derivatives $(\partial^2 B_k/\partial z^2)$ have to be taken into account.

B. Exact analysis

As the SVAA cannot be applied in several situations it is of some interest to calculate the SHG field in a more exact way, assuming only that the fundamental field is not substantially depleted. The calculation has to be carried out numerically, but this is actually not a serious disadvantage. Namely, we have not yet specified the procedure to get the field inside the liquid crystal at the fundamental frequency, given the incoming field. This also has to be carried out numerically, except in the Maugain limit, that is, if the helical pitch is much longer than the wavelength. We will see that the exact procedure of finding the fundamental field inside the sample is very similar to the calculation of the SHG field, so there is actually little point to use the SVAA to get quantitative results.

We start with the inhomogeneous wave equation (5), assuming $E(\vec{r},2\omega) \ll E(\vec{r},\omega)$ so that the nonlinear polarization on the right-hand side of Eq. (5) is independent of $\vec{E}(\vec{r},2\omega)$. We first have to express it in terms of the waves incident on the Sm-C^* slab. It is given by the right-hand side of Eq. (18). The amplitudes A_k of the excited eigenwaves are determined by the boundary conditions for the field at both the surfaces, that is, the transverse components and their derivatives have to be continuous across the boundary. As all phase relations are kept, the result will also include the interference effects arising from multiple reflections inside the slab, which are in a realistic case non-negligible, as we will see.

In some interesting cases of phase matching the waves propagating in both directions are needed, so we assume there is a field $\vec{E}_L(\vec{r},\omega)=\vec{E}_{L0}e^{ik_0 z}$ incident from the left and a field $\vec{E}_R(\vec{r},\omega)=\vec{E}_{R0}e^{-ik_0 z}$ from the right-hand side of the sample. In order to be able to satisfy the boundary conditions we must also keep the two waves of unknown amplitude $\vec{F}_L(\vec{r},\omega)=\vec{F}_{L0}e^{-ik_0 z}$ and $\vec{F}_R(\vec{r},\omega)=\vec{F}_{R0}e^{ik_0 z}$ that are transmitted and reflected from both sides of the slab.

It is advantageous to organize the computation in the following way, similar to the Berreman formalism [24]. Let all the fields be expressed in the circular basis. From the two transverse components of the internal field $\vec{E}^{\rm tr}(\vec{r},\omega)$ we form a four-component vector by adding the derivatives as the third and fourth components:

$$\mathcal{E}=\left[E_+,E_-,\frac{\partial E_+}{\partial z},\ \frac{\partial E_-}{\partial z}\right] \tag{30}$$

This vector can be expressed in terms of a four-component vector of the excited amplitudes of the eigenwaves $\mathcal{A}=[A_k]$ as

$$\mathcal{E}=\mathbf{P}(z)\mathcal{A}, \tag{31}$$

where $\mathbf{P}(z)$ is a 4×4 matrix containing the eigenwaves (8) as the first two rows and their derivatives as the third and fourth rows:

$$\mathbf{P}(z)=\begin{bmatrix} E_{k_n,+} \\ E_{k_n,-} \\ (k_n+q_0)E_{k_n,+} \\ (k_n-q_0)E_{k_n,-} \end{bmatrix}, \quad n=1\ldots,4. \tag{32}$$

Similar four-component vectors are constructed also from the incoming fields $\vec{E}_L(\vec{r},\omega)$ and $\vec{E}_R(\vec{r},\omega)$:

$$\begin{aligned} \mathcal{E}_L&=[E_{L,+},E_{L,-},k_0E_{L,+},k_0E_{L,-},], \\ \mathcal{E}_R&=[E_{R,+},E_{R,-},-k_0E_{R,+},-k_0E_{R,-}]. \end{aligned} \tag{33}$$

The corresponding unknown fields emanating from both faces can be constructed by first forming a four-dimensional vector

$$\mathcal{F}=[F_{L,+},F_{L,-},F_{R,+},F_{R,-}]. \tag{34}$$

Then the two vectors corresponding to

$$\begin{aligned} \mathcal{F}_L&=[F_{L,+},F_{L,-},-k_0F_{L,+},-k_0F_{L,-}], \\ \mathcal{F}_R&=[F_{R,+},F_{R,-},k_0F_{R,+},k_0F_{R,-}] \end{aligned} \tag{35}$$

can be obtained from $\mathcal{F}$ by

$$\mathcal{F}_L=\mathbf{S}_L\mathcal{F}, \quad \mathcal{F}_R=\mathbf{S}_R\mathcal{F}, \tag{36}$$

where $\mathbf{S}_L$ and $\mathbf{S}_R$ are matrices

$$\begin{aligned} \mathbf{S}_R&=\begin{bmatrix} 1 & 0 & 0 & 0 \\ 0 & 1 & 0 & 0 \\ -k_0 & 0 & 0 & 0 \\ 0 & -k_0 & 0 & 0 \end{bmatrix}, \\ \mathbf{S}_R&=\begin{bmatrix} 0 & 0 & 1 & 0 \\ 0 & 0 & 0 & 1 \\ 0 & 0 & k_0 & 0 \\ 0 & 0 & 0 & k_0 \end{bmatrix}. \end{aligned} \tag{37}$$

After these somewhat lengthy preparations, we can write down the boundary conditions at both faces in a very compact form

$$\mathbf{P}(0)\mathcal{A}=\mathbf{S}_L\mathcal{F}+\mathcal{E}_L, \quad \mathbf{P}(L)\mathcal{A}=\mathbf{S}_R\mathcal{F}+\mathcal{E}_R. \tag{38}$$

The unknown vector $\mathcal{F}$ is given by the solution of the linear system

$$[\mathbf{P}(L)\mathbf{P}^{-1}(0)\mathbf{S}_L-\mathbf{S}_R]\mathcal{F}=\mathcal{E}_R-\mathbf{P}(L)\mathbf{P}^{-1}(0)\mathcal{E}_L \tag{39}$$

Then the internal field $\mathcal{A}$ is expressed as

$$\mathcal{A}=\mathbf{P}^{-1}(0)[\mathbf{S}_L\mathcal{F}+\mathcal{E}_L] \tag{40}$$

The above procedure is very suitable to implement on a computer. It gives us exactly the internal field $\vec{E}^{\rm tr}(\vec{r},\omega)$ and as a by-product also the field reflected and transmitted on the slab, including the Bragg reflection at the frequency gap.

We proceed by evaluating the induced polarization at the second-harmonic frequency 2ω using the right-hand side of Eq. (18). Its two circular components have an $e^{iq_0 z}$ and an $e^{-iq_0 z}$ spatial dependence. In addition, according to Eq. (18), there is a sum of terms with exponential factors of the form $e^{i[k'(\omega)+k''(\omega)]z}$, where, in general all four values of $k'(\omega)$ and $k''(\omega)$ are present. One of these terms may be equal to or near an allowed value for $k(2\omega)$ and therefore (nearly) phase matched. Such a term will obviously dominate the SHG field. As we have assumed that there is no depletion, we can treat each term with a particular phase factor $e^{ik(2\omega)z}$ separately.

It is computationally advantageous to write the inhomogeneous wave equation (5) in a space-dependent basis

$$\tilde{e}_+=\vec{e}_+e^{iq_0 z}, \quad \tilde{e}_-=\vec{e}_-e^{-iq_0 z}. \tag{41}$$

Writing the SHG field in the form

$$\vec{E}^{\rm tr}(\vec{r},2\omega)=u_+(\vec{r},2\omega)\tilde{e}_++u_-(\vec{r},2\omega)\tilde{e}_-, \tag{42}$$

the wave equation (5) takes the form

$$\frac{\partial^2 u_\pm}{\partial z^2} \mp 2iq_0 \frac{\partial u_\pm}{\partial z} + [(2\omega)^2 - q_0^2]u_\pm + \alpha(2\omega)^2 u_\mp = P_\pm e^{i[k'(\omega)+k''(\omega)]z} \tag{43}$$

where

$$P_\pm e^{i[k'(\omega)+k''(\omega)]z} = -\left(\frac{2\omega}{c}\right)^2 A_{k'} A_{k''} \vec{e}^{\,*}_\pm \chi^{(2)}_{\rm tr} : \vec{E}^{\rm tr}_{k,\omega} \vec{E}^{\rm tr}_{k'',\omega}. \tag{44}$$

Introducing

$$\mathcal{U} = \left[u_+, u_-, \frac{\partial u_+}{\partial z}, \frac{\partial u_-}{\partial z} \right] \tag{45}$$

and

$$\mathcal{P} = [0,0,P_+,P_-], \tag{46}$$

we write Eq. (43) in the form

$$\frac{\partial \mathcal{U}}{\partial z} + \mathbf{M}\mathcal{U} = \mathcal{P} e^{i[k'(\omega)+k''(\omega)]z}, \tag{47}$$

where $\mathbf{M}$ is the matrix

$$\mathbf{M} \begin{bmatrix} 0 & 0 & -1 & 0 \\ 0 & 0 & 0 & -1 \\ (2\omega)^2 - q_0^2 & \alpha & -2iq_0 & 0 \\ \alpha & (2\omega)^2 - q_0^2 & 0 & -2iq_0 \end{bmatrix}. \tag{48}$$

The solution of this equation is the sum of a particular solution $\mathcal{U}_p$ and a solution of the homogeneous equation $\mathcal{U}_h$, which can be written in a form analogous to Eq. (31):

$$\mathcal{U}_h = \mathbf{\Pi}(z)\mathcal{B}, \tag{49}$$

where $\mathbf{\Pi}(z)$ is the matrix of the eigensolutions of the homogeneous equation and $\mathcal{B}$ are the unknown amplitudes.

The particular solution of Eq. (46) can be written in the form

$$\mathcal{U}_p = \mathbf{K}\mathbf{\Pi}^{-1}(z)\mathcal{P} e^{i[k'(\omega)+k''(\omega)]z}, \tag{50}$$

where $\mathbf{K}$ is a diagonal matrix. When $k'(\omega)+k''(\omega)$ is not equal to one of the eigenvalues $k(2\omega)$, its elements are

$$K_{nn} = \frac{1}{i[k'(\omega)+k''(\omega)-k_n(2\omega)]}, \quad n = 1\ldots,4. \tag{51}$$

When $k'(\omega)+k''(\omega) = k_m(2\omega)$, that is, in a phase-matched situation, the mth element of $\mathbf{K}$ becomes

$$K_{mm} = \frac{z}{k_m(2\omega)}, \tag{52}$$

leading to the expected linear growth of a phase-matched SHG wave.

In order to complete the calculation, we have to satisfy the boundary conditions. As there are no fields incident on the slab at the second-harmonic frequency 2ω (these would be present in the case of a parametric process), we have only two SHG waves radiated into the free space on the left and right of the slab with amplitudes $\vec{G}_L(\vec{r},2\omega) = \vec{G}_{L0} e^{-ik_0 z}$ and $\vec{G}_R(\vec{r},2\omega) = \vec{G}_{R0} e^{ik_0 z}$. We combine them as in Eq. (34) into a four-component vector $\mathcal{G}$. The boundary conditions are then written in the form

$$\mathbf{\Pi}(0)\mathcal{B} + \mathcal{U}_p(0) = \mathbf{S}_L \mathcal{G}, \quad \mathbf{\Pi}(L)\mathcal{B} + \mathcal{U}_p(L) = \mathbf{S}_R \mathcal{G} \tag{53}$$

From these equations the sought amplitudes $\vec{G}_{L0}$ and $\vec{G}_{R0}$ of the second-harmonic waves are obtained as the solution of the linear system

$$[\mathbf{\Pi}(L)\mathbf{\Pi}^{-1}(0)\mathbf{S}_L - \mathbf{S}_R]\mathcal{G} = \mathbf{\Pi}(L)\mathbf{\Pi}^{-1}(0)[\mathcal{U}_p(L) - \mathcal{U}_p(0)]. \tag{54}$$

Some results of the exact analysis are described in the following section.

IV. PHASE MATCHING

The power conversion from the fundamental to the second-harmonic beam in thick samples is efficient only when the phase-matching condition $\Delta k = 0$ is realized. In such situations the analysis is simple because the corresponding combination of the eigenmodes strongly dominates in the SHG process. As the dispersion relation $k(\omega)$ in the helical Sm-C^* structure is quite complex a variety of different phase-matched combinations is expected. Their number is considerably larger than in the homogeneous Sm-C^* structure, where at most two types of phase matching can exist.

By taking into account all the possible values of $k'(\omega)$, $k''(\omega)$, and $k(2\omega)$, the equation $\Delta k = 0$ results in 18 qualitatively different phase-matched combinations of the eigenmodes. When considering a definite sign of the material color dispersion this number reduces to 10. The 10 combinations corresponding to the case of positive color dispersion $[\overline{\varepsilon(2\omega)} > \overline{\varepsilon(\omega)}]$ are summarized in Table I and are shown schematically in Fig. 1. Their relation to the helical wave vector q_0 is given in the third column of the table, where it is evaluated within the approximation $k = \pm(k_0\sqrt{\overline{\varepsilon}} \pm q_0)$, which is reasonable everywhere except for the very high frequencies and close to the gap (for modes 2 and 3). The fourth column shows the frequency region where the combinations can be realized. Seven of the ten phase-matched combinations appear when the frequency of the optical fields lies within or in the vicinity of the band gap, while three of them take place when $\omega, 2\omega \gg \omega_B$, that is, when the wavelength of the optical beams is much shorter than the helical pitch p.

The experimental arrangements corresponding to the particular phase-matched combinations can be classified into three categories. The first category includes the combinations (a), (c), and (f) from Fig. 1, which are realized when $\omega, 2\omega \gg \omega_B$ and describe the usual arrangements where the fundamental beam enters the sample from only one side and the second-harmonic beam copropagates out of the sample with the fundamental beam. From this point of view the combinations (c) and (f) are analogous to the type-I and type-II phase matchings in the homogeneous Sm-C^* structure, while the combination (a) represents a different type related

TABLE I. Phase-matched combinations of the Bloch wave vectors in the Sm-C^* material with the positive color dispersion. The third column gives the corresponding relations between the average material refractive indices $\sqrt{\varepsilon(2\omega)}, \sqrt{\varepsilon(\omega)}$ and the helical wave vector q_0. The fourth column gives the frequency region where certain combinations are realized. The last column gives the effective nonlinear optical susceptibility calculated within the approximation of the circularly polarized eigenmodes. For an interpretation of the modes associated with different branches see Fig. 1.

Label	Combination	Relation with q_0	Region of the realization	Approximate effective susceptibility
(a)	$k_1^{2\omega}=2k_1^{\omega}$	$\frac{2\omega}{c}[\sqrt{\varepsilon(2\omega)}-\sqrt{\varepsilon(\omega)}]\approx q_0$	$2\omega,\omega\gg\omega_B$	$g_1(\theta)$
(b)	$k_1^{2\omega}=2k_3^{\omega}$	$\frac{2\omega}{c}[\sqrt{\varepsilon(2\omega)}+\sqrt{\varepsilon(\omega)}]\approx q_0$	$2\omega,\omega<\omega_B$	$g_1(\theta)$
(c)	$k_2^{2\omega}=2k_1^{\omega}$	$\frac{2\omega}{c}[\sqrt{\varepsilon(2\omega)}-\sqrt{\varepsilon(\omega)}]\approx 3q_0$	$2\omega,\omega\gg\omega_B$	
(d)	$k_2^{2\omega}=2k_3^{\omega}$	$\frac{2\omega}{c}[\sqrt{\varepsilon(2\omega)}+\sqrt{\varepsilon(\omega)}]\approx 3q_0$	$2\omega>\omega_B,\omega<\omega_B$	$g_3(\theta)$
(e)	$k_1^{2\omega}=k_1^{\omega}+k_3^{\omega}$	$\frac{2\omega}{c}[\sqrt{\varepsilon(2\omega)}]\approx q_0$	$2\omega\cong\omega_B$	$g_1(\theta)$
(f)	$k_2^{2\omega}=k_1^{\omega}+k_2^{\omega}$	$\frac{2\omega}{c}[\sqrt{\varepsilon(2\omega)}-\sqrt{\varepsilon(\omega)}]\approx q_0$	$2\omega,\omega\gg\omega_B$	
(g)	$k_2^{2\omega}=k_1^{\omega}+k_3^{\omega}$	$\frac{2\omega}{c}[\sqrt{\varepsilon(2\omega)}]\approx 3q_0$	$2\omega\cong 3\omega_B$	$g_3(\theta)$
(h)	$k_2^{2\omega}=k_3^{\omega}+k_4^{\omega}$	$\frac{2\omega}{c}[\sqrt{\varepsilon(2\omega)}+\sqrt{\varepsilon(\omega)}]\approx q_0$	$2\omega,\omega<\omega_B$	$g_2(\theta)$
(i)	$k_2^{2\omega}=k_2^{\omega}+k_3^{\omega}=0$	$\frac{2\omega}{c}[\sqrt{\varepsilon(2\omega)}]\approx q_0$	2ω at the band edge	
(j)	$k_2^{2\omega}=k_1^{\omega}+k_4^{\omega}=0$	$\frac{2\omega}{c}[\sqrt{\varepsilon(2\omega)}]\approx q_0$	2ω at the band edge	

to the helical modulation. When the anisotropy α of the Sm-C^* material is large compared to the color dispersion it can happen that the ''usual'' combinations (c) and (f) cannot be realized at all.

The second category, which is related to the combinations (b), (d), and (h) from Fig. 1, represents the situations with counterpropagating fundamental and second-harmonic beams. The third category, which includes the combinations (e), (g), (i), and (j) from Fig. 1 correspond to the ''mixed'' arrangements where the fundamental beams that enter the sample from both sides are required and the second-harmonic beams propagate out of the sample in one or both directions. For these two categories the momentum associated with the optical field is not conserved, but its excess or deficit is transferred to the material. These are the so-called umklapp SHG processes [11,12]

In the last column of the Table I the approximate effective nonlinear optical susceptibility for some combinations is given. It was calculated by assuming that the eigenmodes are circularly polarized, that is, taking $f_k, f_{k'}, f_{k''}=0$ or $\pm\infty$ in Eq. (8). This assumption is very reasonable for combinations (b), (d), (e), (g), and (h) and less appropriate for case (a). Within this assumption the effective nonlinear susceptibility (22) of a particular phase-matched combination is related to a single circular component of the tensor $\chi_{\mathrm{tr}}^{(2)}$ and is expressed in terms of the functions $g_i(\theta)$, which are given in the Appendix. The relation between the $g_i(\theta)$ and the amplitude of the second-harmonic field is

$$B_k(z)=\frac{(2\omega/c)^2}{(k\pm q_0)}\, g_i(\theta) A_{k'} A_{k''} z. \tag{55}$$

This relation can be used to estimate the approximate output SHG power emanating from the helical Sm-C^* structure in a particular experimental arrangement.

To calculate the expected SHG power more accurately the exact calculation procedure described in Sec. III has to be performed. It can be applied to any of the ten phase-matched situations and also to the non-phase-matched cases. Figure 2 shows the second-harmonic intensity for the linearly polarized fundamental beam with fundamental frequency about $0.5\omega_B$ as a function of frequency or q_0. The strong phase-matched peak is the result of four separate phase-matched combinations: (i), (j), (e), and the inverse of (e) with branches 2 and 4 of the dispersion spectrum. In each case, the necessary fundamental beam traveling in the direction opposite to the incoming beam is generated by the reflection at the sample surface. For either the forward or backward propagating second-harmonic beam, about 75% of the amplitude is the result of the combinations (i) and (j) and 25% of the combinations (e) and their equivalent. The total SHG intensity is a coherent sum of the partial contributions, so it is very important to know their relative phases, which is possible only with the exact calculation.

Figure 3 shows the total SHG intensity as a function of sample thickness or equivalently q_0 for phase-matching case (g), which is at fundamental frequency $\omega\approx 1.5\omega_B$. The

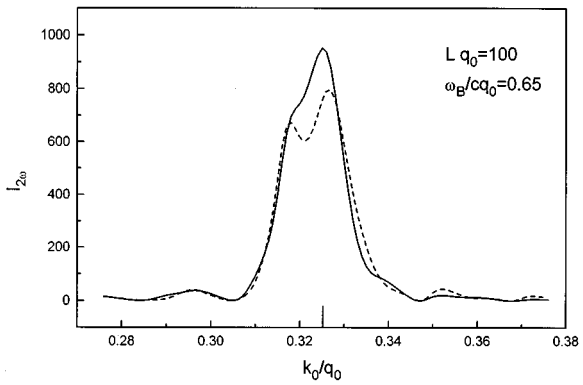

FIG. 2. Total transmitted (solid line) and reflected (dashed line) SHG intensity for the linearly polarized fundamental beam with frequency $\omega \approx 0.5\omega_B$ as a function of k_0 or q_0. The contributing phase-matched combinations are the combinations (i), (j), and (e) and the inverse of (e).

rather complicated fringe pattern is the result of the interference of the waves at ω and 2ω due to the multiple reflections at the sample surfaces. The chosen frequency is phase matched, so the average over the oscillations is proportional to the square of the sample thickness L^2, as indicated by the dotted line. Again, this fringe pattern cannot be obtained by the SVAA.

Figure 4 shows the SHG intensity for phase-matched case (g) as a function of frequency, calculated by SVAA and exactly. The difference in this case is primarily due to the interference effects and therefore also depends on the choice of sample thickness.

V. DISCUSSION

One of the prominent properties of the optical SHG in the helical Sm-C^* phase is that the interference oscillations of the second-harmonic field as given by Eq. (23) originate primarily from the helical modulation and not from the color dispersion of the optical dielectric tensor as in the case of the homogeneous media. The color dispersion is important for the SHG only in the first category of the phase-matched combinations [combinations (a), (c), and (f) from Fig. 1],

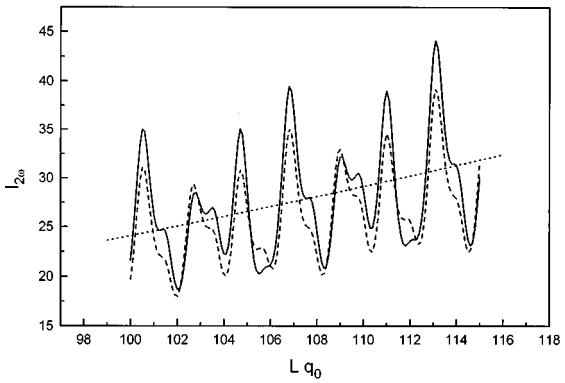

FIG. 3. Total reflected (solid line) and transmitted (dashed line) SHG intensity for the linearly polarized fundamental beam as a function of sample length at $\omega \approx 1.5\omega_B$ [phase-matching case (g)]. The dotted line corresponds to the L^2 dependence.

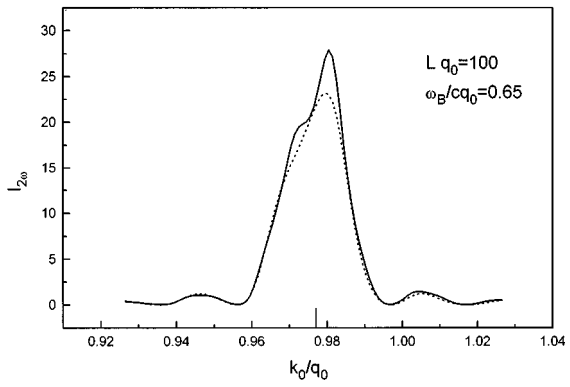

FIG. 4. SHG intensity for the linearly polarized input beam at $\omega \approx 1.5\omega_B$ as a function of k_0 or q_0, calculated by the SVAA (dotted line) or by the exact procedure (solid line).

which corresponds to the situations where the optical wavelength is much shorter than the helical pitch p, that is, the so-called Mauguin limit of the beam propagation [21]. All the other phase-matched combinations are quite insensitive to the color dispersion and might be considered as examples of the nonlinear Bragg reflection from the helical structure. They have no analogy in the homogeneous Sm-C^* phase and therefore represent different possibilities for efficient SHG in the helical Sm-C^* material.

Due to the different order of nonlinearity some qualitatively other phenomena can be observed when studying SHG instead of the THG (or field-induced SHG) in the helical liquid-crystalline materials [12–15]. The main distinctions appear when the harmonic frequency is close to the edge of the selective reflection band. In this case, as shown originally by Belyakov and Shipov, a remarkable ''additional'' enhancement of the SHG or THG can appear [18,25,26] The ''additional'' enhancement means that the amplitude of the harmonic field $B_k(z)$ increases faster than linearly with the sample thichness. When considering the THG this enhancement is possible only if a definite relation between the helical wave vector q_0 and the color dispersion $\overline{\varepsilon}(3\omega)-\overline{\varepsilon}(\omega)$ is valid. For the analogous enhancement of the SHG, on the contrary, there are no additional requirements on the color dispersion and therefore the phenomenon is much more likely to be experimentally observed. The effect of enhancement is described with the phase-matched combinations (i) and (j) from Fig. 1.

The geometries related to the phase matching in the region of the selective reflection band can explain the experimental results of Kajikawa *et al.* [16] and Furukawa *et al.* [17], who have observed an increase of the SHG when the helical pitch of the Sm-C^* material was tuned to the second-harmonic wavelength. The fundamental beam was linearly polarized and entered the sample from one side only. The second-harmonic beam of equal intensity appeared in the forward as well as the backward direction with respect to the incident beam. According to our analysis, the linearly polarized incident beam results in both types of fundamental eigenmodes within the sample. Both of the eigenmodes are then partially back reflected from the back surface of the sample and consequently the combination of the forward and the backward propagating modes enables the realization of the combinations (i), (j), (e), and the inverse of (e) simulta-

neously. The theoretical calculation of the SHG intensity for such a case is shown in Fig. 2 and is in very good agreement with the experimental results.

The experiments of Kajikawa *et al.* and Furukawa *et al.* are, to our knowledge, the only experimental investigation of the optical SHG in the helically twisted Sm-C^* phase performed until now. The reason that such studies are so rare with respect to the SHG studies in the homogeneous unwound Sm-C^* phase is probably the weak dependence of the Sm-C^* helical pitch on temperature. A considerable variation of the pitch, which is required in order to observe different phase-matched combinations by using a fixed fundamental frequency, appears only close to the temperature of the phase transition from the Sm-C^* to the Sm-A or the cholesteric phase. In this region the nonlinear susceptibility of the material rapidly decreases with increasing temperature and the corresponding low SHG intensity prevents good quality measurements. This problem may be overcome by tuning the wavelength of the laser instead of the periodicity of the material. Another possibility is also to vary the helical pitch not by changing the temperature of the sample but rather by changing the concentration of the left- and right-handed compounds at temperatures far below the phase transition. In this respect different mixtures of Sm-C^* materials exhibiting a large nonlinear optical susceptibility and at the same time having the capability to vary the pitch by varying the composition would be very appropriate to optimize the SHG signal. A MATHEMATICA package that gives exact numerical solutions for the SHG field in the case of the wave propagation along the Sm-C^* helical axis in various experimental geometries can be found on the Internet at location http://optlab.ijs.si/lcpro

APPENDIX: COMPONENTS OF THE $\chi^{(2)}$ IN VARIOUS COORDINATE SYSTEMS

In the laboratory system; for the Cartesian base

$$\chi_{xxx}=-3[\chi_{112}\cos^2\theta+\chi_{332}\sin^2\theta+\chi_{132}\sin^2\theta]\cos^2\varphi\sin\varphi-\chi_{222}\sin^3\varphi,$$

$$\chi_{xxy}=[\chi_{112}\cos^2\theta+\chi_{332}\sin^2\theta+\chi_{132}\sin2\theta]\times\cos\varphi(3\cos^2\varphi-2)+\chi_{222}\cos\varphi\sin^2\varphi,$$

$$\chi_{xxz}=\tfrac{1}{2}[\chi_{112}\sin2\theta-\chi_{332}\sin2\theta-2\chi_{132}\cos2\theta]\sin2\varphi,$$

$$\chi_{xyy}=-[\chi_{112}\cos^2\theta+\chi_{332}\sin^2\theta+\chi_{132}\sin2\theta]\sin\varphi(3\sin^2\varphi-2)-\chi_{222}\cos^2\varphi\sin\varphi,$$

$$\chi_{yyy}=3[\chi_{112}\cos^2\theta+\chi_{332}\sin^2\theta+\chi_{132}\sin2\theta]\cos\varphi\sin^2\varphi+\chi_{222}\cos^3\varphi,$$

$$\chi_{yyz}=-\tfrac{1}{2}[\chi_{112}\sin2\theta-\chi_{332}\sin2\theta-2\chi_{132}\cos2\theta]\sin2\varphi,$$

$$\chi_{zzx}=-[\chi_{112}\sin^2\theta+\chi_{332}\cos^2\theta-\chi_{132}\sin2\theta]\sin\varphi,$$

$$\chi_{zzy}=[\chi_{112}\sin^2\theta+\chi_{332}\cos^2\theta-\chi_{132}\sin2\theta]\cos\varphi,$$

$$\chi_{yxz}=-\tfrac{1}{2}[\chi_{112}\sin2\theta-\chi_{332}\sin2\theta-2\chi_{132}\cos2\theta]\cos^2\varphi,$$

$$\chi_{zzz}=0,$$

where

$$\varphi=(2\pi z/p)=q_0 z.$$

In the laboratory system, for the circular base,

$$\chi_{+++}=-(\chi_{++-})^*=\chi_{-++}=-(\chi_{---})^*=-\frac{1}{(\sqrt{2})^3}(\chi_{xxx}-i\chi_{xxy}+\chi_{xyy}-i\chi_{yyy}),$$

$$\chi_{+--}=-(\chi_{-++})^*=-\frac{1}{(\sqrt{2})^3}(\chi_{xxx}+3i\chi_{xxy}-3\chi_{xyy}-i\chi_{yyy}),$$

$$\chi_{+-0}=(\chi_{-+0})^*=-(\chi_{0++})^*=-\chi_{0--}=-\tfrac{1}{2}(\chi_{xxz}-\chi_{yyz}+2i\chi_{xyz}),$$

$$\chi_{++0}=\chi_{--0}=-\chi_{0+-}=\tfrac{1}{2}(\chi_{xxz}+\chi_{yyz}),$$

$$\chi_{+00}=-(\chi_{-00})^*=-\chi_{00-}=(\chi_{00+})^*=-\frac{1}{\sqrt{2}}(\chi_{xzz}+i\chi_{yzz}),$$

$$\chi_{000}=\chi_{zzz}.$$

The components χ_{ijk} in the circular base are symmetric only with respect to the permutations of the last two indices. By incorporating the previously given relations in the Cartesian base these expressions transform to

$$\chi_{+++}=-(\chi_{++-})^*=\chi_{-++}=-(\chi_{---})^*=-\frac{i}{(\sqrt{2})^3}(\chi_{112}\cos^2\theta+\chi_{332}\sin^2\theta+\chi_{123}\sin2\theta+\chi_{222})e^{-iq_0z},$$

$$\chi_{+--}=-(\chi_{-++})^*=-\frac{i}{(\sqrt{2})^3}(3\chi_{112}\cos^2\theta+3\chi_{332}\sin^2\theta+3\chi_{123}\sin2\theta-\chi_{222})e^{3iq_0z},$$

$$\chi_{+-0}=(\chi_{-+0})^*=-(\chi_{0++})^*=-\chi_{0--}=\frac{1}{2}[(\chi_{112}-\chi_{332})\sin2\theta-2\chi_{123}\cos2\theta]e^{2iq_0z},$$

$$\chi_{+00}=-(\chi_{-00})^*=-\chi_{00-}=(\chi_{00+})^*=-\frac{i}{\sqrt{2}}(\chi_{112}\sin^2\theta+\chi_{332}\cos^2\theta-\chi_{123}\sin2\theta)e^{iq_0z},$$

$$\chi_{++0}=\chi_{--0}=\chi_{0+-}=\chi_{000}=0.$$

The components of the tensor of the transverse nonlinear susceptibilty $\chi^{(2)}_{\mathrm{tr}}$ are then given by

$$\chi_{\mathrm{tr},+++}=-(\chi_{\mathrm{tr},---})^{*}=\left(\chi_{+++}-2\chi_{++0}\frac{a}{\sqrt{2}}e^{-iq_0z}+\chi_{+00}\frac{a^2}{2}e^{-2iq_0z}\right)=ig_1(\theta)e^{-iq_0z},$$

$$\chi_{\mathrm{tr},++-}=-(\chi_{\mathrm{tr},--+})^{*}=\left(\chi_{++-}+\chi_{++0}\frac{a}{\sqrt{2}}e^{+iq_0z}-\chi_{+-0}\frac{a}{\sqrt{2}}e^{-iq_0z}-\chi_{+00}\frac{a^2}{2}\right)=ig_2(\theta)e^{iq_0z},$$

$$\chi_{\mathrm{tr},+--}=-(\chi_{\mathrm{tr},-++})^{*}=\left(\chi_{+--}+2\chi_{+-0}\frac{a}{\sqrt{2}}e^{iq_0z}+\chi_{+00}\frac{a^2}{2}e^{2iq_0z}\right)=ig_3(\theta)e^{3iq_0z},$$

where the functions $g_i(\theta)$ are

$$g_1(\theta)=-\frac{1}{(\sqrt{2})^3}[\chi_{112}(\cos^2\theta+a^2\sin^2\theta)+\chi_{332}(\sin^2\theta+a^2\cos^2\theta)+\chi_{123}(\sin2\theta)(1-a^2)+\chi_{222}],$$

$$g_2(\theta)=\frac{1}{(\sqrt{2})^3}[\chi_{112}(\cos\theta-a\sin\theta)^2+\chi_{332}(\sin\theta+a\cos\theta)^2+\chi_{123}(\sin2\theta+2a\cos2\theta-a^2\sin2\theta)+\chi_{222}],$$

$$g_3(\theta)=\frac{1}{(\sqrt{2})^3}[\chi_{112}(-3\cos^2\theta+2a\sin2\theta-a^2\sin^2\theta)+\chi_{332}(-3\sin^2\theta-2a\sin2\theta-a^2\cos^2\theta)+\chi_{123}(-3\sin2\theta-4a\cos2\theta+a^2\sin2\theta)+\chi_{222}].$$

[1] N. M. Shtykov, M. I. Barnik, L. A. Beresnev, and L. M. Blinov, Mol. Cryst. Liq. Cryst. **124**, 379 (1985).
[2] K. Yoshino, S. Kishio, M. Ozaki, A. Yukoatani, T. Sasaki, and C. Yamanaka, Tech. Rep. Osaka Univ. **37**, 283 (1987).
[3] M. Ozaki, K. Mimoto, and K. Yoshino, Tech. Rep. Osaka Univ. **39**, 217 (1989).
[4] A. Taguchi, Y. Ouchi, H. Takezoe, and A. Fukuda, Jpn. J. Appl. Phys. 2, Lett. **28**, L997 (1989).
[5] M. Ozaki and K. Yoshino, Jpn. J. Appl. Phys. 2, Lett. **28**, L1830 (1989).
[6] J. Y. Liu, M. G. Robinson, K. M. Johnson, and D. Doroski, Opt. Lett. **15**, 267 (1990).
[7] M. Ozaki, M. Utsumi, T. Gotou, K. Daido, and K. Yoshino, Jpn. J. Appl. Phys. 2, Lett. **30**, L1569 (1991).
[8] M. Utsumi, T. Gotou, K. Daido, M. Ozaki, and K. Yoshino, Jpn. J. Appl. Phys. 1 **30**, 2369 (1991).
[9] M. Ozaki, M. Utsumi, T. Gotou, Y. Morita, K. Daido, Y. Sadohara, and K. Yoshino, Ferroelectrics **121**, 259 (1991).
[10] See, for instance, A. Yariv, *Quantum Electronics*, 2nd ed. (Wiley, New York, 1975).
[11] For recent review see, for instance, M. Houé and P. D. Townsend, J. Phys. D **28**, 1747 (1995).
[12] J. W. Shelton and Y. R. Shen, Phys. Rev. Lett. **25**, 23 (1970).
[13] J. W. Shelton and Y. R. Shen, Phys. Rev. Lett. **26**, 538 (1971).
[14] J. W. Shelton and Y. R. Shen, Phys. Rev. A **5**, 1867 (1972).
[15] S. K. Saha, Opt. Commun. **37**, 373 (1981).
[16] K. Kajikawa, T. Isozaki, H. Takezoe, and A. Fukuda, Jpn. J. Appl. Phys. 2, Lett. **31**, L679 (1992).
[17] T. Furukawa, T. Yamada, K. Ishikawa, H. Takezoe, and A. Fukuda, Appl. Phys. B **60**, 485 (1995).
[18] M. Čopič and I. Drevenšek Olenik, Liq. Cryst. **21**, 233 (1996).
[19] D. W. Berreman, Mol. Cryst. Liq. Cryst. **22**, 175 (1973).
[20] O. Parodi, J. Phys. (France) **36**, 22 (1975).
[21] H. P. de Vries, Acta Crystallogr. **4**, 219 (1951).
[22] P. G. de Gennes, *The Physics of Liquid Crystals* (Clarendon, Oxford, 1974).
[23] See, for instance, N. Bloembergen, *Nonlinear Optics* (Benjamin, New York, 1964).
[24] D. W. Berreman, J. Opt. Soc. Am. **62**, 502 (1972).
[25] V. A. Belyakov and N. V. Shipov, Phys. Lett. **86A**, 94 (1981).
[26] V. A. Belyakov and N. V. Shipov, Zh. Eksp. Teor. Fiz. **75**, 1589 (1978) [Sov. Phys. JETP **55**, 647 (1982)].